Quantitative estimation of thermoelectric contributions in spin pumping signals through microwave photoresistance measurements

Jun Cheng, Kang He, Man Yang, Qi Liu, Rui Yu, Liang Sun, Jinjun Ding, Bingfeng Miao, Mingzhong Wu, and H. F. Ding

Phys. Rev. B **103**, 014415 — Published 12 January 2021

DOI: 10.1103/PhysRevB.103.014415

Quantitative Estimation of Thermoelectric Contributions in Spin Pumping Signals through Microwave Photoresistance Measurements

Jun Cheng[1], Kang He[1], Man Yang[1], Qi Liu[1], Rui Yu[1], Liang Sun[1, 2], Jinjun Ding[3], Bingfeng Miao[1, 2]*, Mingzhong Wu[3], H. F. Ding[1, 2]

[1]*National Laboratory of Solid State Microstructures and Department of Physics, Nanjing University, Nanjing, P.R. China*

[2]*Collaborative Innovation Center of Advanced Microstructures, Nanjing, P.R. China*

[3]*Department of Physics, Colorado State University, Fort Collins, CO 80523, USA*

*Corresponding author. E-mail: bfmiao@nju.edu.cn

Abstract

Spin pumping is a technique widely used to generate pure spin current and characterize the spin-charge conversion efficiency of heavy metals. Upon the microwave excitation, the sample may also be heated and the parasitic thermoelectric signals could contaminate the spin pumping results. Owning to their identical angular dependences with respect to the magnetic field, it is difficult to isolate one from the other. In this work, we present a quantitative method to separate thermoelectric contributions from spin pumping signals in both Py($Ni_{80}Fe_{20}$)/Pt and YIG($Y_3Fe_5O_{12}$)/Pt bilayers through microwave photoresistance measurements. We find that the microwave absorption indeed can raise the temperature of samples, resulting a field-dependent thermoelectric hysteresis loop. However, the additional heat dissipation due to the resonant precession of the magnetization in the ferromagnet is negligibly small as compared to the measured spin pumping signal. Thus, we conclude that the spin pumping signal is free of any detectable thermoelectric contributions.

Introduction

Recently, spintronic research shifts interests from spin-polarized current to pure spin current. In conductors, pure spin current can deliver maximum spin angular momentum with minimum electrons [1,2]. In magnetic insulators, spin information can transfer in the form of collective motion of magnetic moments, i.e., spin waves [3-5], without any moving charge carriers. Utilizing pure spin current generates less Joule heat and thus has less power consumption, as compared to the spin polarized current. Spin Hall effect (SHE) [6,7], spin pumping [8-10] and spin Seebeck effect (SSE) [11,12] based techniques have been developed to generate pure spin current. Among various mechanisms, spin pumping has the unique interface spin current characterizing capability, thus has also been widely used to characterize the spin Hall angle and spin diffusion length of heavy metals [13-16]. Upon the application of the microwave excitation and with an appropriate external magnetic field, the magnetic moments in a ferromagnet can be driven into a coherent precession (ferromagnetic resonance, FMR) [17]. This non-equilibrium magnetization dynamic in a ferromagnet acts as the source for an angular momentum flow, which pumps a spin current into its neighboring non-magnetic layer [8-10]. Due to the lack of net charge current, the detection of pure spin current mainly relies on the inverse spin Hall effect (ISHE) in metals with strong spin-orbit coupling, which converts spin current into charge current with density $\boldsymbol{J}_{\mathrm{C}} = \theta_{\mathrm{SH}} (2e/\hbar) \boldsymbol{J}_{\mathrm{S}} \times \boldsymbol{\sigma}$ [10]. Here, θ_{SH} is the spin Hall angle which characterizes the efficiency of the spin-charge conversion, e is the electronic charge, $\hbar$ is the reduced Planck constant, $\boldsymbol{J}_{\mathrm{S}}$ represents the spin current density, and $\boldsymbol{\sigma}$ denotes the spin direction parallel with the equilibrium magnetization of the ferromagnet. Because of the orthogonal relation, perpendicular flowing of spin current with spin polarization along the y-direction results in an in-plane charge current flows along the x-direction (see coordinates in Fig. 1). In an open-circuit, a spin pumping voltage $\boldsymbol{E}_{\mathrm{SP}} \propto \boldsymbol{J}_{\mathrm{S}} \times \boldsymbol{\sigma}$ is obtained [Fig. 1(a)].

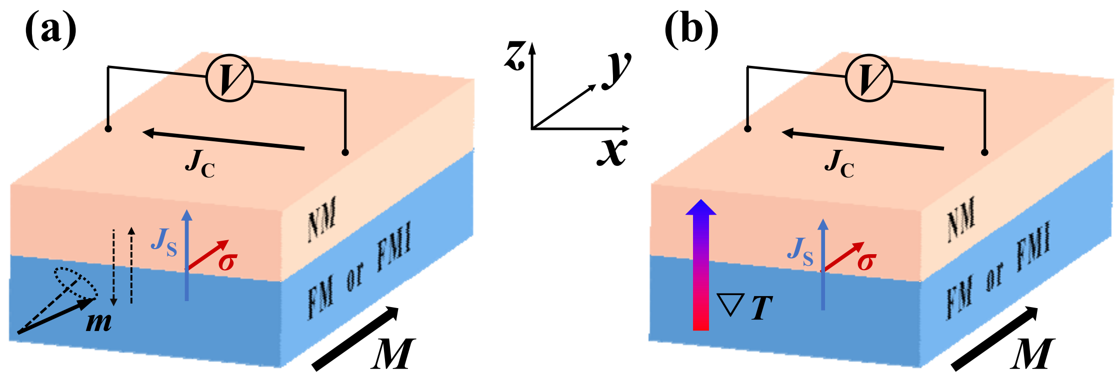

FIG. 1. Schematic illustrations of (a) spin pumping (b) longitudinal spin Seebeck effect.

Spin pumping requires a microwave to excite the precession of the magnetic moments. However, the microwave irradiation may also bring possible thermoelectric artifacts. Both the eddy currents in conductors and magnon–phonon scattering in ferromagnet could heat the samples [18-22]. Typically, for devices with a thin film deposited on a thick substrate, the temperature increase might establish a perpendicular temperature gradient, which gives rise to thermoelectric signals such as the Nernst effect, the longitudinal spin Seebeck effect (LSSE) [12], the anomalous Nernst effect (ANE) [23-25] and the spin-dependent Seebeck effect (SdSE) [26] when the ferromagnetic layer is conducting. Therefore, the spin pumping signals are potentially contaminated with thermoelectric contributions [27,28]. The Nernst effect can be easily excluded since it is independent with the magnetic field, and the SdSE typically is very small [29,30]. However, the separation of the LSSE and ANE contributions from the spin pumping signal is not straightforward. Under an out-of-plane (perpendicular) temperature gradient, the LSSE enables a pure spin current injected vertically from the ferromagnet into the heavy metal and detected as a transverse thermal voltage $\boldsymbol{E}_{\mathrm{LSSE}} \propto \nabla_z T \times \boldsymbol{\sigma}$ through the ISHE, where $\boldsymbol{\sigma}$ is parallel with the magnetization $\boldsymbol{M}$ of the ferromagnet, as depicted in

Fig. 1(b). When the ferromagnet is conducting, under the same $\nabla_z T$, the ANE of $\boldsymbol{E}_{\mathrm{ANE}} \propto \nabla_z T \times \boldsymbol{M}$ also gives rise to a transverse voltage. One can readily find that the spin pumping, LSSE, and ANE voltages all share the same symmetry with the same angular dependence, hence inseparable and additive. Furthermore, if the thermoelectric contributions are dominating, the measured signal in the ferromagnet/heavy metal structure may even fail to denote the spin Hall angle sign of the heavy metal [31]. Therefore, it is important to develop a quantitative method to separate thermoelectric contributions in the spin pumping experiments.

In this work, we present a universal and quantitative method to obtain the thermoelectric contributions in spin pumping voltage via the assistance of the microwave-photoresistance measurements. We apply this method on two typical systems, i.e., Py($Ni_{80}Fe_{20}$)/Pt and YIG($Y_3Fe_5O_{12}$)/Pt bilayers, and find that the microwave radiation indeed can raise the sample temperatures and create a perpendicular temperature gradient. This vertical temperature gradient induces a sizable thermal voltage due to the LSSE and the ANE near zero magnetic field, which acts as a background for spin pumping signals at higher fields. However, the additional heat dissipation due to magnon-phonon scattering at the FMR condition is negligibly small, in consistent with previous findings [27,28]. This conclusion is further supported by the field-dependent microwave absorption measurement using a vector network analyzer. Therefore, we conclude that the thermoelectric contributions are little, if any, as compared with the spin pumping signal in our measurement geometry.

Experiments and results

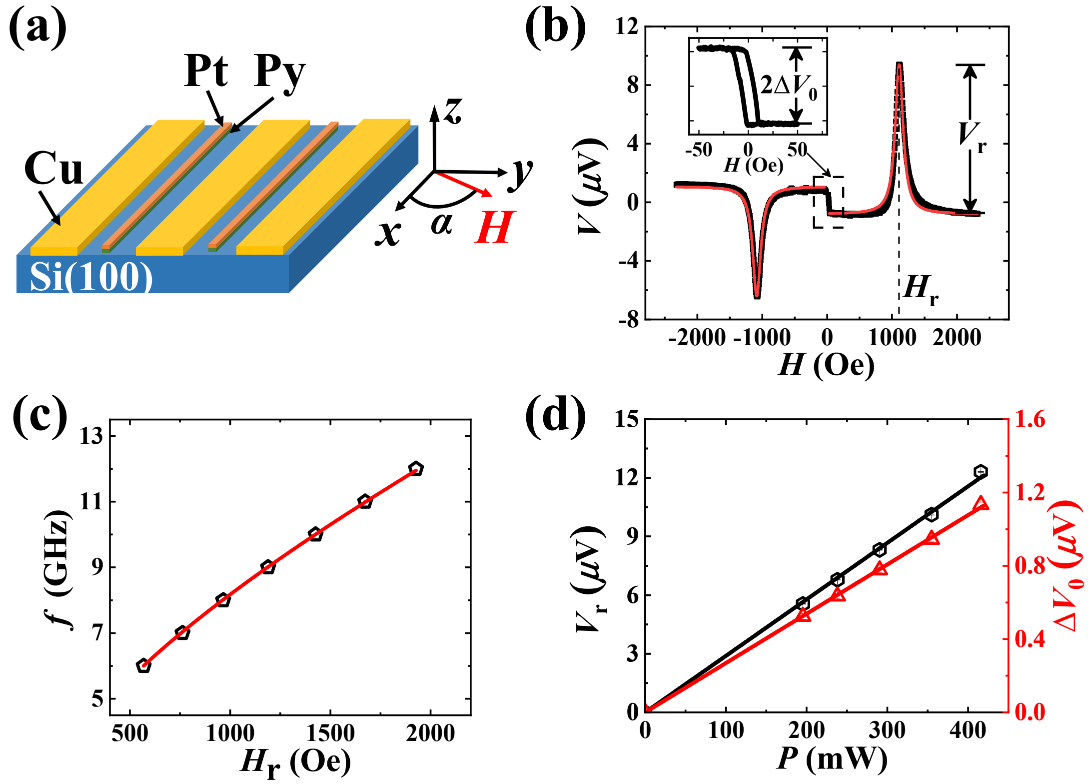

FIG. 2. (a) Schematic illustration of the experimental setup for spin pumping measurements of Py/Pt bilayer. (b) Field-dependent voltage for a Py(6 nm)/Pt(3 nm) bilayer stripe with 8.5 GHz microwave irradiation, where the magnetic field is applied along the *y*-direction. The black symbols represent the experimental data, and the red lines are the Lorentz line fittings. The inset presents the zoomed-in feature near zero magnetic field. $2\Delta V_0$ denotes the difference of the voltage background for the positive and negative fields. (c) Microwave frequency f dependent resonance field H_r. Black circles are the experimental data, and the red line is the fitting with Kittel equation. (d) Microwave input power dependent V_r (black hexagon, left scale) and ΔV_0 (red triangle, right scale). The lines are linear fittings.

We perform the measurements with two representative ferromagnet/normal metal bilayer structures, Py/Pt and YIG/Pt, where Py is a metal and YIG is an insulator. The Py(6 nm)/Pt(3 nm) bilayer with the length l=2 mm and the width w=20 μm is deposited on the thermally oxidized Si substrate (total thickness is 0.5 mm, SiO_2 is ~300 nm) and glass substrate (1 mm thick). For the YIG/Pt system, we first deposit a 25-nm-thick YIG film on a (111)-$Gd_3Ga_5O_{12}$ (GGG) substrate (0.5 mm thick) and perform post-annealing at 800°C at atmosphere for 4 hours. Then, a 5-nm Pt stripe (l=1.53 mm and w=40 μm) is deposited on the YIG continuous film. A 100-nm copper coplanar waveguide (CPW) with a 50-Ω characteristic impedance is fabricated to introduce the microwaves, with the Pt stripes integrated into the slots between the signal and ground lines of the CPW [Fig. 2(a)]. In this configuration, the microwave magnetic field h_{rf} is primarily along the z-direction. In order to achieve high sensitivity, a lock-in technique is used. We modulate the microwave with a Transistor-Transistor Logic (TTL) signal with a frequency of 8.3 kHz and measure the voltage as the function of an external magnetic field applied in the xy-plane with an angle α with respect to the x-direction, as marked in Fig. 2(a). All films are deposited by magnetron sputtering at room temperature, with the thickness calibrated by x-ray reflection measurements. And all measurements are performed at room temperature except for the R-T curve. For the measurement of Py/Pt bilayer, the microwave frequency is 8.5 GHz with a 355-mW power unless specified.

Figure 2(b) presents the voltage obtained across the two ends of the Py/Pt bilayer stripe, where the magnetic field is applied along the y-direction. In this geometry, the spin rectification due to the microwave induction current and oscillating anisotropic magnetoresistance (AMR) is minimized. It shows that a pair of voltage peak and dip appears at ±1.1 kOe with a symmetric Lorentz line shape, indicating its pure spin current origin. The different amplitudes in the spin pumping signals for $\pm H$ [Fig. 2(b)] in our measurement are caused by different precession angles of the magnetization ($\boldsymbol{M}$) under magnetic fields with opposite directions. After normalizing the measured V_{sp} with their corresponding in-plane and out-of-plane precession angles produce, the normalized signals will become almost identical [32]. Interestingly, the background for the positive and negative magnetic fields has a sizable difference, marked as $2\Delta V_0$ [see Fig. 2(b)]. The voltage at low fields is asymmetric in H, with a field dependence following the magnetization curve of Py. The data show a coercivity smaller than 10 Oe [see Fig. 2(b) inset]. This zero-field step signal may result from non-resonant spin rectification of the Py layer [33], and/or microwave heating induced ANE of the Py layer and LSSE of the Py/Pt bilayer. While the non-resonant spin rectification is proportional with the magnetic field derivative of resistance $\mathrm{d}R/\mathrm{d}H$, it disappears after the magnetization is saturated [33]. Since no discernible difference of voltage background is observed for zero field and high fields, we conclude that the voltage step near zero field here is a thermoelectric contribution.

Now we turn to the signal at the resonance field, H_r. As depicted in Fig. 2c, the f-dependent H_r can be well described by the Kittle equation, which yields the saturation magnetization $4\pi M_0$(Py) to be 7.53 kOe. We further define the amplitude of the Lorentzian line fitting at the positive resonance field as V_r, which is typically attributed to the spin pumping signal only. However, if the temperature enhancement due to magnon-phonon scattering under the resonance condition is non-negligible, thermoelectric signals from the ANE and the LSSE will also be involved. As mentioned above, the signals from ANE, LSSE, and spin pumping all share the same symmetry, it is difficult to distinguish them by routing methods. Moreover, we further find that both ΔV_0 and V_r are linearly proportional to the input microwave power [Fig. 2(d)]. Thus, it is not possible to distinguish them from their power dependences, either.

As discussed above, ΔV_0 is of pure thermoelectric origin, while V_r at the resonance state may have both spin pumping and thermoelectric contributions. Thus, it is pivotal to find a parameter which links zero-field ΔV_0 and possible thermoelectric contributions in V_r. A natural option is the resistance of the Py/Pt bilayer, which relates to the sample temperature as well as the temperature gradient. Figure 3(a) shows the temperature-dependent resistance change with respect to the resistance at 300 K. Since the sample is a metallic bilayer, its resistance shows a linear increase with the temperature. The fitting yields a slope of 7.12(±0.02) Ω/K. Thus, it could serve as a sensitive tool to probe the temperature change.

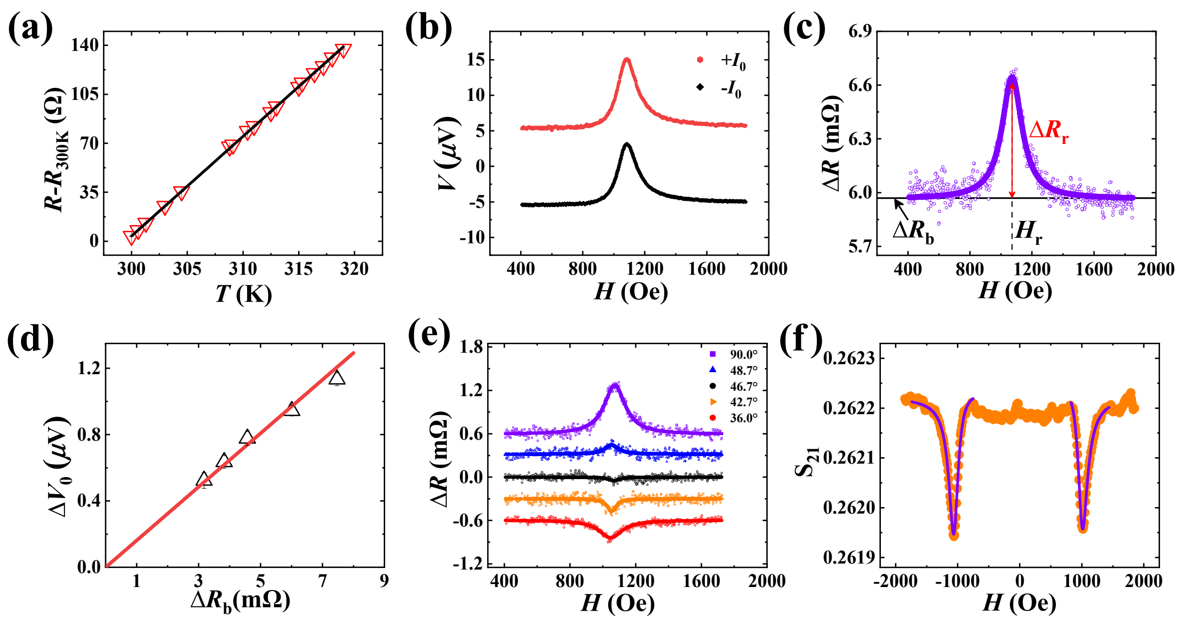

FIG. 3. (a) R-T curve of a Py(6 nm)/Pt(3 nm) bilayer near room temperature, with a slope of 7.12(± 0.02) Ω/K. R_{300K} = 8.86 kΩ. (b) Magnetic field-dependent voltages with dc current $+I_0$ (+0.9 mA, red curve) and $-I_0$ (−0.9 mA, black curve) for the Py/Pt sample, respectively. (c) The resistance difference ΔR of the Py/Pt bilayer between microwave on and off states. (d) Linear relation between the thermoelectric ground ΔV_0 and the resistance difference background ΔR_b. (e) Magnetic field dependent ΔR for different α. The curves are shifted for clarity. (f) Magnetic field-dependent S_{21} parameter data for a "7 mm×7 mm" Py(6 nm)/Pt(3 nm) film.

We further investigate the change of the sample resistance during the spin pumping measurement. In order to obtain this, we feed the sample with a small current and measure the voltage change as a function of the external field. We note that the microwave is modulated with an 8.3-kHz TTL signal, and the lock-in detection picks up the voltage difference between the microwave on and off states with the same frequency. Therefore, the resistance change reflects the temperature difference between the microwave on and off states (in ms), instead of the real temperature of the Py/Pt bilayer. Figure 3(b) presents the H dependent voltages with dc current $+I_0$ (+0.9 mA, red curve) and $-I_0$ (−0.9 mA, black curve), respectively. The magnetic field is applied along the y-axis ($\alpha = 90°$). We obtain the resistance difference of the Py/Pt bilayer between the microwave on and off states by $\Delta R = [V(+I_0) - V(-I_0)]/2I_0$, as presented in Fig. 3(c). The ΔR curve has a non-zero background ΔR_b and a peak with the amplitude ΔR_r coincide with the resonance field H_r. At the magnetic field away from H_r, ΔR_b comes from the heating due to the microwave only, and increases with the power. Thus, we find a linear relation between ΔV_0 [the thermoelectric background signal depicted in Fig. 2(b)] and ΔR_b (the resistance increase background value), with a slope 0.162 μV/mΩ [Fig. 3(d)]. If we further obtain the additional heating-induced resistance increase at the FMR condition, the thermoelectric contributions in the spin pumping signal can be calculated. However, aside from the temperature increase via magnon–phonon scattering at FMR, the resistance change ΔR has another origin which also needs to be addressed. As a magnetic material, Py has AMR with $R_{\|} > R_{\perp}$, where $R_{\|}$ and $R_{\perp}$ are the longitudinal ($M \| I$) and transverse ($M \perp I$) magnetoresistance, respectively. At the FMR, the magnetization precession alters the angle of the magnetization with respect to the dc current, resulting in a change of the time-averaged AMR. This is termed as the microwave photoresistance ΔR_{MW}, and its angular dependence is given by: [34]

$$\Delta R_{\mathrm{MW}} = R_{\mathrm{A}}(-\alpha_1^2 \cos 2\alpha - \beta_1^2 \cos^2 \alpha)/2 \quad (1)$$

Here, R_A is the difference between $R_{\parallel}$ and $R_{\perp}$, which is about 36.19 Ω for our Py/Pt sample, and α_1, β_1 are the amplitudes of in-plane and out-of-plane precession angles of the magnetization, respectively. According to the FMR theory, the in-plane and out-of-plane precession angles have a relation of $\alpha_1/\beta_1 = \sqrt{1+M_0/H_{\mathrm{r}}}$ [16,34], with M_0 being the saturation magnetization of the ferromagnet. Equation (1) shows that ΔR_{MW} is α-dependent, and disappears at

$$|\cos\alpha| = \sqrt{\frac{H_{\mathrm{r}} + M_0}{3H_{\mathrm{r}} + 2M_0}} \quad (2)$$

For the Py/Pt bilayer, we find that ΔR_{MW} equals to zero when α=46.7°. Thus, the residual resistance enhancement at the FMR condition with α=46.7° can be attributed to the temperature increase only.

Figure 3(e) presents the ΔR versus H curves in the vicinity of the resonance field H_r for different α. The curves are shifted for clarity. When α is varied from 90° to 36°, ΔR_r changes from positive to negative and disappears at around 46.7°. For α=46.7°, ΔR is almost a flat curve. The fitting yields $\Delta R_r = -0.05(\pm 0.008)$ mΩ. Combined with the calibration curve presented in Fig. 3(d), we estimate the thermoelectric signal to be $<9.4\times10^{-3}$ μV [the product of the slope in Fig. 3(d) and the measure ΔR_r]. Thus, thermal contributions in spin pumping voltage for Py/Pt are < 0.09% [0.009 μV/10.20 μV, with 10.20 μV is the value of the symmetrical line fitted by the positive magnetic field part in Fig. 2(b)], which can be safely neglected. The slope of R-T curve is 7.12 Ω/K [Fig. 3(a)], and the microwave on-off resistance change ΔR_b is 6.01 mΩ [Fig. 3(d)] for 355-mW microwave power， thus we estimate the ΔT due to off-resonance microwave heating to be $8.43(\pm 0.48)\times10^{-4}$ K [the ratio of the measured ΔR_b and the slope in Fig. 3(a)], and the additional ΔT at FMR condition due to magnon-phonon scattering is $< 8.15\times10^{-6}$ K.

It is important to emphasize that both ΔR and ΔT are not the resistance and temperature differences compared with room temperature after the microwave irradiation. Instead, they correspond to the quasi-steady resistance and temperature differences between microwave on and off state, which is modulated by lock-in amplifier with 8.3 kHz. It is also interesting to note that the thermoelectric signal at FMR state is about two orders' magnitude smaller than that of the off-resonance state. In order to understand this, we perform S parameter S_{21} using a vector network analyzer (VNA). S_{21} characterizes the transmission insertion loss of the whole devices, obtained through the ratio of transmitted and input microwave. Due to the small volume of stripe line sample, the FMR absorption dip is not observed. Therefore, a Py(6nm) /Pt(3nm) bilayer film of lateral dimension 7 mm×7 mm is grown to achieve a reasonable signal-to-noise ratio. In consistent with the spin pumping measurements, microwave absorption due to FMR occurs at ±1.1 kOe [Fig. 3(f)]. We note that the additional absorption due to FMR is relatively small compared with the S_{21} parameter background, around 0.1%. This explains why thermoelectric signal for ANE/LSSE has sizable contribution near zero magnetic field, while it is negligibly small at FMR condition for Py/Pt bilayer system. And we expect that thermoelectric contribution plays important role only if the magnetic contrast in S_{21} parameter is comparable with non-magnetic background.

Recently, aside from magnetic metals, magnetic insulators also attract growing interests from spintronics community. Due to its ability to accommodate pure spin currents without charge carriers, magnetic insulators have great potential for low-power spintronics application. Among various magnetic insulators, YIG has the unique attributes of ultra-low damping [35], long spin diffusion length [3]. It has been widely investigated in spin Hall magnetoresistance (SMR) [36,37], spin Seebeck effect [12], spin pumping [38,39] and photon-magnon coupling [40,41] etc. Therefore, it is intriguing to study the thermoelectric contributions in spin pumping experiment of YIG/Pt system.

Figure 4(a) illustrates our setup of YIG/Pt measurements. Figure 4(b) presents the spin pumping curve under the irradiation of 5 GHz microwave with 355 mW, where the magnetic field is applied along the *y*-axis (α=90°). A 20-μV voltage with opposite polarity is observed at ±1.2 kOe. Fitting the resonance magnetic field H_r dependent microwave frequency [Fig. 4(c)] with Kittel equation yields the saturation magnetization $4\pi M_0$ = 1.40 kOe, which is similar as the reported value for YIG film [42]. Because of the small half-line width of YIG film, the peak of spin pumping curve here is much sharper than that of Py/Pt system. Although there may exist magnetic proximity effect in the YIG/Pt bilayer system [43], the possible ANE has been shown to be negligible [44]. Thus, the voltage step near zero-field ΔV_0 mainly comes from the LSSE of YIG/Pt bilayer.

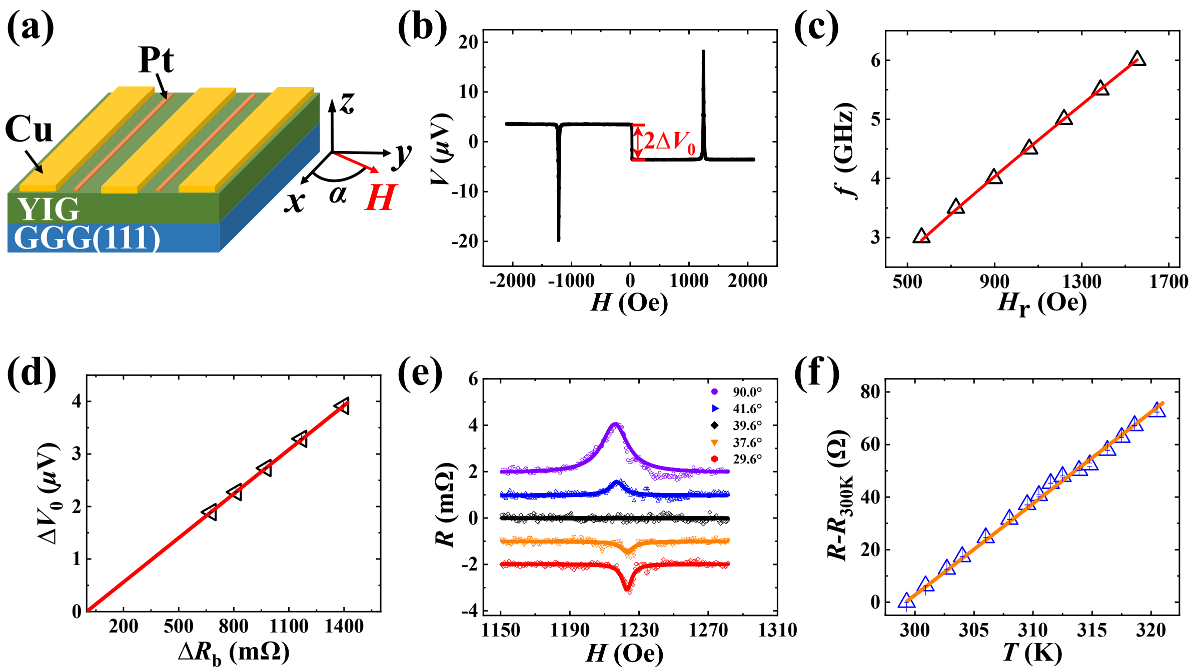

FIG. 4. (a) Schematic illustration of the experimental setup for spin pumping measurement of YIG/Pt bilayer. (b) Field-dependent voltage for a YIG/Pt(5 nm) bilayer stripe with 5 GHz microwave irradiation, where the magnetic field is applied along the *y*-direction. (c) Ferromagnetic resonance field dependent microwave frequency. (d) ΔV_0 as the function of ΔR_b. The red line is the linear fitting

with a slope of 2.8×10^{-3} μV/mΩ. (e) H-dependent ΔR for different α. The curves are shifted for clarity. (f) The R-T curve of YIG/Pt(5 nm) near room temperature, where the slope is around 3.48(±0.04) Ω/K. $R_{300\mathrm{K}} = 3.72$ kΩ.

By measuring the spin pumping curve with 0 mA, and ±0.3 mA under microwave with different power, we obtain the corresponding zero-field voltage step ΔV_0 and resistance difference ΔR_{b} at off-resonance state for the YIG/Pt bilayer. The calibration curve for ΔV_0 versus ΔR_{b} for the YIG/Pt bilayer is presented at Fig. 4(d). ΔV_0 is linearly proportional with ΔR_{b}, with a slope of 2.8×10^{-3} μV/mΩ. Although YIG is insulating, the resistance in the YIG/Pt depends on the direction of the magnetization of the underlying YIG with respect to the current due to the SMR effect [36,37]. When the magnetization of YIG rotates within the xy-plane, SMR has exactly the same angular dependence as AMR. Thus, YIG/Pt also has microwave photoresistance ΔR_{MW} with the same symmetry as that of Py/Pt, described by Eq. (1). With the measured parameters of our YIG/Pt sample, we calculate that ΔR_{MW} disappears at $\alpha = 39.6°$. Any detected resistance change at this specific angle can be attributed to the heating due to magnon-phonon scattering at the FMR condition. We present the ΔR_{r} of YIG/Pt at the vicinity of H_{r} of YIG for different magnetic field directions in Fig. 4(e). The polarity of ΔR_{r} changes from positive at $\alpha = 90.0°$ to negative at $\alpha = 29.6°$, vanishing at $\alpha = 39.6°$ with a noise level < 0.3 mΩ. We note the small deviation of resonance field H_{r} (< 8 Oe) at different angles is due to the misalignment between magnetic field and sample plane. In combination with the calibration curve in Fig. 4(d), we obtain the thermoelectric contributions of YIG/Pt to be $< 8.4\times10^{-4}$ μV, which is around 4~5 order's smaller than the spin pumping voltage. Therefore, in our geometry, thermoelectric contributions in spin pumping signal of YIG/Pt are also negligibly small. The resistance difference background ΔR_b is 1170 mΩ for YIG/Pt under 355-mW microwave irradiation [same condition for Fig. 4(b)], in combination with the slope of *R*-*T* curve, 3.48(±0.04) Ω/K [Fig. 4(f)], we estimate the temperature difference is 0.34 K near zero magnetic field. Meanwhile, we estimate the additional temperature increase at the FMR condition is less than 8.62×10^{-5} K.

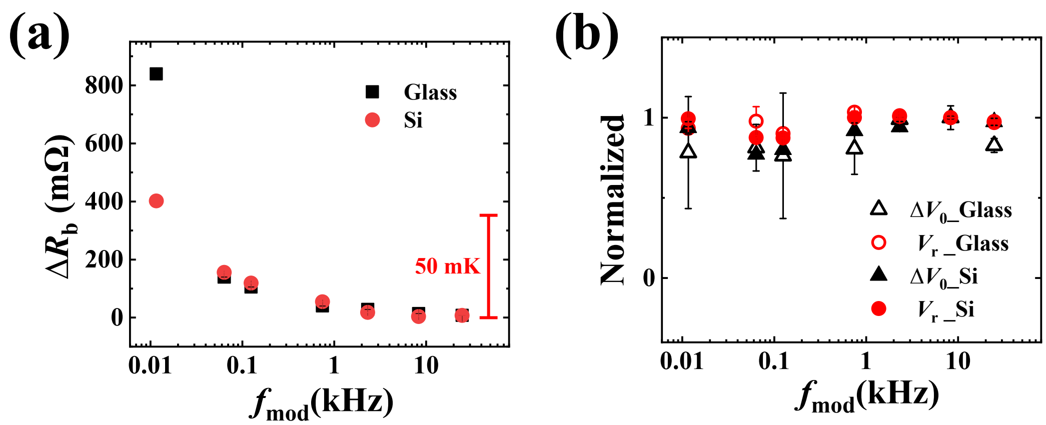

FIG. 5. Lock-in modulation frequency dependent ΔR_b (a), and ΔV_0 and V_r (b) for Py/Pt deposited on Si and glass substrates. All voltages have been normalized to the value with f_{mod} =8.3 kHz. The applied microwave is 8.5 GHz in frequency and 355-mW in power.

Discussion

We further study the influence of substrate thermal conductivity and the lock-in modulation frequency on the thermoelectric effect. In addition to thermally oxidized Si, we also deposit a Py(6 nm)/Pt(3 nm) bilayer onto a glass substrate, whose thermal conductivity is about 2 orders of magnitude smaller than that of Si. Figure. 5(a) presents the background resistance difference ΔR_b as function of lock-in frequency f_{mod} on both the Si and the glass substrate. With decreasing f_{mod}, ΔR_b increases sharply at low frequency. This can be explained by the relative slow bulk thermal relaxation, similar feature had been reported in Ref. [45]. For the Si substrate, we estimate the ΔT

due to off-resonance microwave heating to be 56.4 mK for 11.6 Hz of f_{mod}, almost 67 times large as that of 8.3 kHz. Although the microwave power applied on Py layer deposited on the glass substrate is smaller due to the low microwave transmission efficiency, ΔR_{b} for glass substrate is larger than that of thermally oxidized Si substrate. Therefore, the global temperature enhancement is larger for low thermal conductivity substrate. In addition, we expect that temperature increase for thicker ferromagnet should be larger as the absorbed microwave enhances thus producing more heating. The much higher lock-in frequency and thinner ferromagnet qualitatively explain the observed smaller temperature increase in this study as compared with those reported in previous works [22,46]. Interestingly, we find the thermoelectric background ΔV_0 for Py/Pt bilayer are almost f_{mod} in-dependent on both the Si and the glass substrates [Fig. 5(b)]. This implies that interfacial temperature gradient can be established with a fast speed. This observation is consistent with temporal evolution study of spin Seebeck effect, where the interfacial temperature gradient is found to be stable within 1 μs, while the global temperature itself needs several ms to saturate [47]. And the lock-in frequency ($<10^8$ Hz) independent spin Seebeck effect for Pt/YIG (thin film) was also reported [48].

Although we focus our study on the thermoelectric contributions of the measured spin pumping signal with out-of-plane microwave magnetic field in this manuscript, our method is not limited to this specific geometry. As long as the angular dependence of the microwave photoresistance ΔR_{MW} and microwave absorption at FMR condition (proportional with the square of microwave magnetic field component that is perpendicular to the magnetization of ferromagnet) is different, our method will be effective. For instance, when h_{rf} is along the y-direction, the microwave absorption at FMR condition is proportional to $\cos^2\alpha$, while the angular dependence of ΔR_{MW} is still

$\Delta R_{\mathrm{MW}} = R_{\mathrm{A}}(-\alpha_1^2 \cos 2\alpha - \beta_1^2 \cos^2 \alpha)/2$ [34]. We note that the in-plane and out-of-plane precession angles of the magnetization α_1, β_1 are external field direction dependent in this geometry. However, the relation $\alpha_1/\beta_1 = \sqrt{1 + M_0/H_{\mathrm{r}}}$ is always maintained. Thus, ΔR_{MW} disappears at $\alpha = \arccos\sqrt{\frac{H_{\mathrm{r}} + M_0}{3H_{\mathrm{r}} + 2M_0}}$, where the additional resistance increase at the FMR condition can be attributed to the thermal effect. With the calibrated curve for voltage background at non-resonant condition, one can obtain the thermoelectric contributions in spin pumping signal as well. In addition, it is also very interesting to apply our approach to investigate thermoelectric contributions in the spin-torque ferromagnetic resonance technique [49,50], where the microwave current is directly injected into the sample and the thermal effect might be stronger.

Summary

In this work, we present a quantitative method to obtain the thermoelectric contributions in spin pumping signals. Benefiting from their different angular dependence on the magnetization direction, we can isolate the resistance increase due to magnon-phonon scattering at the FMR condition from the microwave photoresistance. In combination with the calibrated curve for non-resonant voltage background, we further quantitatively obtain the thermoelectric contributions at the FMR condition. Although sizable LSSE/ANE are observed near zero magnetic field for Py/Pt and YIG/Pt, they are negligible in resonant spin pumping signals. The influence of the substrate thermal conductivity and the lock-in modulation frequency are also discussed. Our work also demonstrates that spin pumping is a reliable technique to investigate pure spin current behavior, no matter the ferromagnet is a conductor or an insulator.

Acknowledgement

This work was supported by the National Key R&D Program of China (Grant No. 2018YFA0306004 and 2017YFA0303202), the National Natural Science Foundation of China (Grants No. 51971110, No. 11974165, No. 11734006, No. 11727808), and the Natural Science Foundation of Jiangsu Province (Grant No. BK20190057). Work at CSU was supported by the U.S. National Science Foundation under Grants No. EFMA-1641989 and No. ECCS-1915849.

References

[1] S. A. Wolf, D. D. Awschalom, R. A. Buhrman, J. M. Daughton, S. von Molnár, M. L. Roukes, A. Y. Chtchelkanova, and D. M. Treger, Science **294**, 1488 (2001).
[2] I. Zutic, J. Fabian, and S. Das Sarma, Rev. Mod. Phys. **76** (2004).
[3] Y. Kajiwara, K. Harii, S. Takahashi, J. Ohe, K. Uchida, M. Mizuguchi, H. Umezawa, H. Kawai, K. Ando, K. Takanashi, S. Maekawa, and E. Saitoh, Nature **464**, 262 (2010).
[4] A. V. Chumak, V. I. Vasyuchka, A. A. Serga, and B. Hillebrands, Nat. Phys. **11**, 453 (2015).
[5] M. Collet, X. de Milly, O. D. Kelly, V. V. Naletov, R. Bernard, P. Bortolotti, J. Ben Youssef, V. E. Demidov, S. O. Demokritov, J. L. Prieto, M. Munoz, V. Cros, A. Anane, G. de Loubens, and O. Klein, Nat. Commun. **7**, 10377 (2016).
[6] J. E. Hirsch, Phys. Rev. Lett. **83**, 1834 (1999).
[7] S. F. Zhang, Phys. Rev. Lett. **85**, 393 (2000).
[8] Y. Tserkovnyak, A. Brataas, and G. E. W. Bauer, Phys. Rev. Lett. **88**, 117601 (2002).
[9] Y. Tserkovnyak, A. Brataas, and G. E. W. Bauer, Phys. Rev. B **66**, 224403 (2002).
[10] E. Saitoh, M. Ueda, H. Miyajima, and G. Tatara, Appl. Phys. Lett. **88**, 182509 (2006).
[11] K. Uchida, S. Takahashi, K. Harii, J. Ieda, W. Koshibae, K. Ando, S. Maekawa, and E. Saitoh, Nature **455**, 778 (2008).
[12] K. Uchida, H. Adachi, T. Ota, H. Nakayama, S. Maekawa, and E. Saitoh, Appl. Phys. Lett. **97**, 172505 (2010).
[13] O. Mosendz, V. Vlaminck, J. E. Pearson, F. Y. Fradin, G. E. W. Bauer, S. D. Bader, and A. Hoffmann, Phys. Rev. B **82**, 214403 (2010).
[14] A. Azevedo, L. H. Vilela-Leao, R. L. Rodriguez-Suarez, A. F. L. Santos, and S. M. Rezende, Phys. Rev. B **83**, 144402 (2011).
[15] H. L. Wang, C. H. Du, Y. Pu, R. Adur, P. C. Hammel, and F. Y. Yang, Phys. Rev. Lett. **112**, 197201 (2014).
[16] Z. Feng, J. Hu, L. Sun, B. You, D. Wu, J. Du, W. Zhang, A. Hu, Y. Yang, D. M. Tang, B. S. Zhang, and H. F. Ding, Phys. Rev. B **85**, 214423 (2012).
[17] C. Kittel, Phys. Rev. **73**, 155 (1948).
[18] N. Yoshikawa and T. Kato, J. Phys. D: Appl. Phys. **43**, 425403 (2010).
[19] F. L. Bakker, J. Flipse, A. Slachter, D. Wagenaar, and B. J. van Wees, Phys. Rev. Lett. **108**, 167602 (2012).
[20] Z. H. Zhang, Y. S. Gui, L. Fu, X. L. Fan, J. W. Cao, D. S. Xue, P. P. Freitas, D. Houssameddine, S. Hemour, K. Wu, and C.-M. Hu, Phys. Rev. Lett. **109**, 037206 (2012).

[21] T. An, V. I. Vasyuchka, K. Uchida, A. V. Chumak, K. Yamaguchi, K. Harii, J. Ohe, M. B. Jungfleisch, Y. Kajiwara, H. Adachi, B. Hillebrands, S. Maekawa, and E. Saitoh, Nat. Mater. **12**, 549 (2013).

[22] K. Yamanoi, Y. Yokotani, and T. Kimura, Appl. Phys. Lett. **107**, 182410 (2015).

[23] T. Miyasato, N. Abe, T. Fujii, A. Asamitsu, S. Onoda, Y. Onose, N. Nagaosa, and Y. Tokura, Phys. Rev. Lett. **99**, 086602 (2007).

[24] K. Uchida, T. Kikkawa, T. Seki, T. Oyake, J. Shiomi, Z. Y. Qiu, K. Takanashi, and E. Saitoh, Phys. Rev. B **92**, 094414 (2015).

[25] Z. H. Duan, B. F. Miao, L. Suni, D. Wu, J. Du, and H. F. Ding, Ieee Magn Lett **10**, 4501805 (2019).

[26] A. Slachter, F. L. Bakker, J. P. Adam, and B. J. van Wees, Nat. Phys. **6**, 879 (2010).

[27] Y. Huo, F. L. Zeng, C. Zhou, and Y. Z. Wu, Phys. Rev. Appl. **8**, 014022 (2017).

[28] P. Noel, M. Cosset-Cheneau, V. Haspot, V. Maurel, C. Lombard, M. Bibes, A. Barthelemy, L. Vila, and J. P. Attane, J. Appl. Phys. **127**, 163907 (2020).

[29] M. Beens, J. P. Heremans, Y. Tserkovnyak, and R. A. Duine, J. Phys. D: Appl. Phys. **51**, 394002 (2018).

[30] R. Iguchi, A. Yagmur, Y. C. Lau, S. Daimon, E. Saitoh, M. Hayashi, and K. Uchida, Phys. Rev. B **98**, 014402 (2018).

[31] W. W. Lin and C. L. Chien, arXiv :1804.01392.

[32] X. D. Tao, Q. Liu, B. F. Miao, R. Yu, Z. Feng, L. Sun, B. You, J. Du, K. Chen, S. F. Zhang, L. Zhang, Z. Yuan, D. Wu, and H. F. Ding, Sci. Adv. **4**, eaat1670 (2018).

[33] X. F. Zhu, M. Harder, J. Tayler, A. Wirthmann, B. Zhang, W. Lu, Y. S. Gui, and C. M. Hu, Phys. Rev. B **83**, 140402 (2011).

[34] N. Mecking, Y. S. Gui, and C.-M. Hu, Phys. Rev. B **76**, 224430 (2007).

[35] H. C. Chang, P. Li, W. Zhang, T. Liu, A. Hoffmann, L. J. Deng, and M. Z. Wu, IEEE Magn. Lett. **5**, 6700104 (2014).

[36] Y. T. Chen, S. Takahashi, H. Nakayama, M. Althammer, S. T. B. Goennenwein, E. Saitoh, and G. E. W. Bauer, Phys. Rev. B **87**, 144411 (2013).

[37] H. Nakayama, M. Althammer, Y. T. Chen, K. Uchida, Y. Kajiwara, D. Kikuchi, T. Ohtani, S. Geprägs, M. Opel, S. Takahashi, R. Gross, G. E. W. Bauer, S. T. B. Goennenwein, and E. Saitoh, Phys. Rev. Lett. **110**, 206601 (2013).

[38] J. C. Rojas-Sanchez, N. Reyren, P. Laczkowski, W. Savero, J. P. Attane, C. Deranlot, M. Jamet, J. M. George, L. Vila, and H. Jaffres, Phys. Rev. Lett. **112**, 106602 (2014).

[39] C. Hahn, G. de Loubens, O. Klein, M. Viret, V. V. Naletov, and J. Ben Youssef, Phys. Rev. B **87**, 174417 (2013).

[40] L. H. Bai, M. Harder, Y. P. Chen, X. Fan, J. Q. Xiao, and C.-M. Hu, Phys. Rev. Lett. **114**, 227201 (2015).

[41] Y.-P. Wang, J. W. Rao, Y. Yang, P.-C. Xu, Y. S. Gui, B. M. Yao, J. Q. You, and C.-M. Hu, Phys. Rev. Lett. **123**, 127202 (2019).

[42] Y.-M. Kang, S.-H. Wee, S.-I. Baik, S.-G. Min, S.-C. Yu, S.-H. Moon, Y.-W. Kim, and S.-I. Yoo, J. Appl. Phys. **97**, 10A319 (2005).

[43] Y. M. Lu, Y. Choi, C. M. Ortega, X. M. Cheng, J. W. Cai, S. Y. Huang, L. Sun, and C. L. Chien, Phys. Rev. Lett. **110**, 147207 (2013).

[44] T. Kikkawa, K. Uchida, Y. Shiomi, Z. Qiu, D. Hou, D. Tian, H. Nakayama, X. F. Jin, and E.

Saitoh, Phys. Rev. Lett. **110**, 067207 (2013).
[45] Y. S. Gui, N. Mecking, A. Wirthmann, L. H. Bai, and C. M. Hu, Appl. Phys. Lett. **91**, 082503 (2007).
[46] N. Vlietstra, B. J. van Wees, and F. K. Dejene, Phys. Rev. B **94**, 035407 (2016).
[47] M. Agrawal, V. I. Vasyuchka, A. A. Serga, A. Kirihara, P. Pirro, T. Langner, M. B. Jungfleisch, A. V. Chumak, E. T. Papaioannou, and B. Hillebrands, Phys. Rev. B **89**, 224414 (2014).
[48] M. Schreier, F. Kramer, H. Huebl, S. Geprägs, R. Gross, S. T. B. Goennenwein, T. Noack, T. Langner, A. A. Serga, B. Hillebrands, and V. I. Vasyuchka, Phys. Rev. B **93**, 224430 (2016).
[49] L. Q. Liu, T. Moriyama, D. C. Ralph, and R. A. Buhrman, Phys. Rev. Lett. **106**, 036601 (2011).
[50] L. Q. Liu, C. F. Pai, Y. Li, H. W. Tseng, D. C. Ralph, and R. A. Buhrman, Science **336**, 555 (2012).